Gold concentration during polyphase deformation: Insights from Boulanger Project, French Guiana

Brice Lacroix, Dennis Lahondes, Pierre-Jean Hainque, Etienne Le Goff, Dominique Fournier, Alix Hauteville, Blandine Gourcerol, Aurélien Eglinger, Anne-Sylvie André-Mayer

Journal of South American Earth Sciences 146 (2024) 105074

Contents lists available at ScienceDirect

Journal of South American Earth Sciences

journal homepage: www.elsevier.com/locate/jsames

Gold concentration during polyphase deformation: Insights from Boulanger Project, French Guiana

Brice Lacroix [a,b,c,*], Dennis Lahondes [b,d], Pierre-Jean Hainque [b,c], Etienne Le Goff [b], Dominique Fournier [b,d], Alix Hauteville [e], Blandine Gourcerol [f], Aurélien Eglinger [e,g], Anne-Sylvie Andre-Mayer [e]

[a] Department of Geology, Kansas State University, USA
[b] GexplOre, Nancy, France
[c] UMR, 6249, Chrono-Environnement, Université de Franche-Comté, Besançon, France
[d] Reunion Gold Corporation, Longueil, (Quebec), Canada
[e] GeoRessources, Université de Lorraine, Nancy, France
[f] BRGM, 45060, Orléans, France
[g] InnovExplo inc., Longueil, (Quebec), Canada

A B S T R A C T

The Boulanger gold deposit is hosted within the Rhyacian greenstone belts from the Guiana shield located within the North Guiana Through, French Guiana. The Boulanger deposit is characterized by a complex polyphase deformation and mineralization history involving a coaxial shortening phase, D_1, followed by a transcurrent deformation event, D_2. The main ore bodies consist of a series of quartz-tourmaline-pyrite-carbonate extension and shear veins in response to NNE-SSW shortening event (D_1), and adjacent altered host-rocks. The proximal alteration bordering the vein system is characterized by pyrite-tourmaline (main ore assemblage). This shortening event is followed by transcurrent deformation, D_2. Locally, D_2 is expressed by the formation of N020-030 narrow zones (F_2 axial trace) along which D_1 structures are reoriented. The structural analysis performed on both $S_{1/0}$ foliation and on geophysical data interpretation highlights the presence of Type-1 interference patterns. These zones are associated with significant gold enrichment and the presence of a new ore assemblage dominated by pyrrhotite-pyrite. Quantitative structural analysis approach, based on measured foliations ($S_{1/0}$) and gold grade demonstrates that D_2-related folding is associated with important gold endowment. These findings suggest that the characterization of the exact fold interference pattern is fundamental for the targeting of favorable enriched zones at the deposit scale.

1. Introduction

Greenstone belts are areas of great interest as they host numerous mineral deposits including volcanic massive sulphide (VMS), Ni-Cu platinum-group element (PGE) sulphide deposits, and more particularly, orogenic gold deposits, which compose an important source for global gold production (Groves et al., 1998; Poulsen, 2000; Goldfarb et al., 2001). Orogenic gold systems formed in deformed terranes at different geological times (from Paleoarchean to early Cenozoic; Neumayr et al., 1998; Craw and Koons, 1989) and at various crustal levels (from low-grade greenschist to high-grade granulite metamorphic conditions) (e.g., Poulsen, 2000; Goldbarb et al., 2005; Dubbé and Gosselin, 2007). Several decades of active research have almost univocally demonstrated that orogenic gold deposits formed from aqueous-carbonic fluid released during metamorphism through devolatilization reactions in the middle to lower crust (e.g., Cox et al., 1991; Philipps and Powell, 2010; Goldfarb and Groves, 2015). The transfer pathways of mineralizing fluids as well as the trapping mechanisms of gold mineralization are strongly controlled by crustal structures such as faults and/or shear zones (increasing porosity and permeability) (e.g., Voissey et al., 2020) as well as the deformation conditions during late orogenic stages (e.g., Combes et al., 2022). While pre-existing structures predating gold input may be of important control for the early stage of ore deposition (e.g., Chauvet et al., 2019), later deformation phases postdating gold input are significant for remobilization/reconcentration processes (also referred as gold endowment) (e.g., Tomkins and Mavrogenes, 2002). Indeed, as reported by several studies, orogenic gold mineralization is not generally associated with a single tectonic event, but rather benefits from polyphase deformation (e.g., gold grade endowment) (Thébaud et al., 2018; Masurel et al., 2022). This has been especially well documented in orogenic gold deposits from Alaska (Juneau terranes; Goldfarb et al., 2008) where grade endowment is

* Corresponding author. Department of Geology, Kansas State University, USA.
E-mail address: blacroix@ksu.edu (B. Lacroix).

https://doi.org/10.1016/j.jsames.2024.105074
Received 6 March 2024; Received in revised form 4 August 2024; Accepted 6 August 2024
Available online 10 August 2024

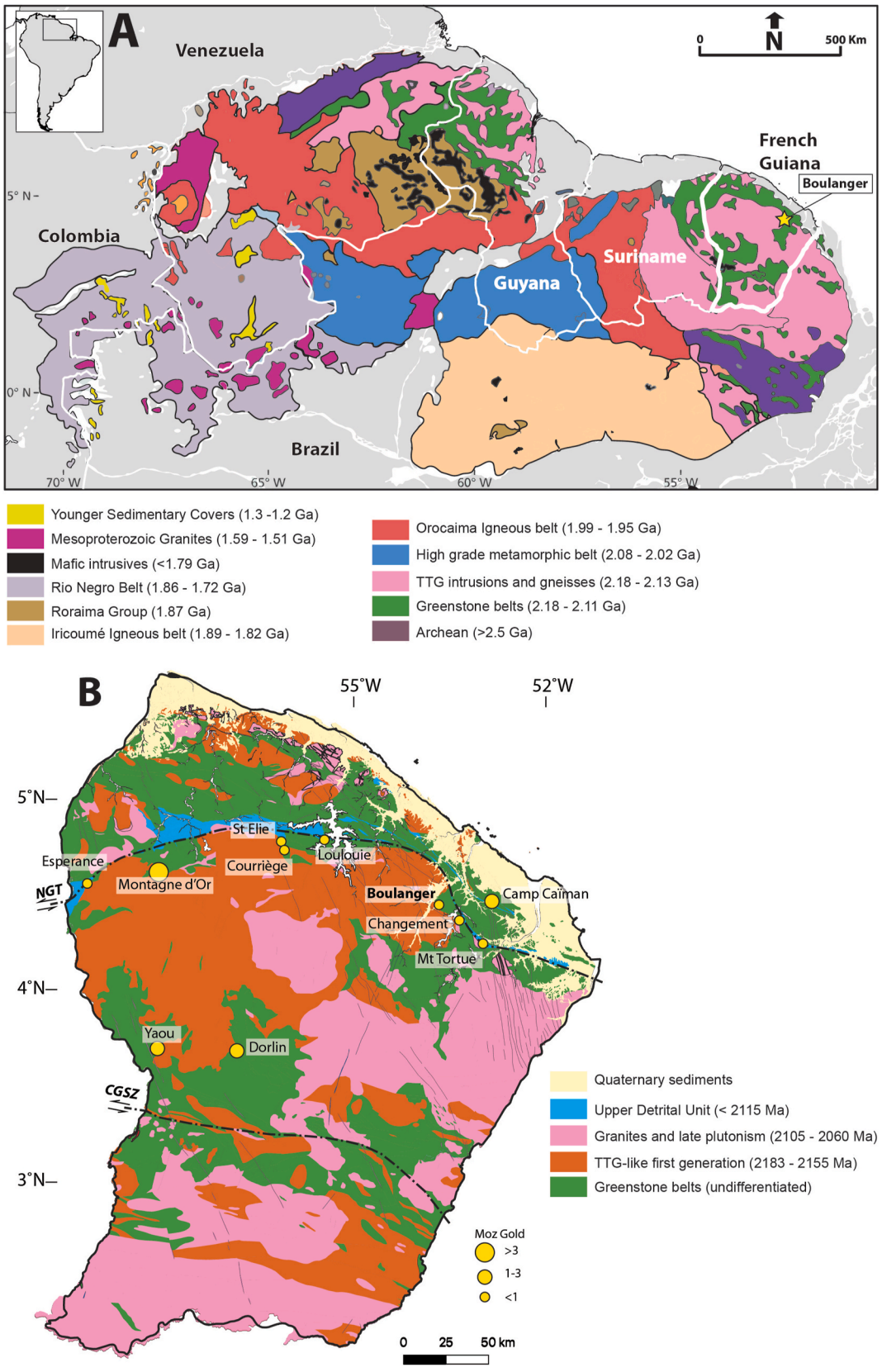

Fig. 1. A. Geology of the Guiana Shield (modified from Kroonenberg et al., 2016; Tedeschi et al., 2020). Yellow stars: location of Boulanger gold-deposit. **B.** Geological map of French Guiana with location of the main Au deposits (Modified from Delor et al., 2003; Combes et al., 2022).

linked to post-subduction transpressive deformation, (e.g., during strike slip reactivation of reverse crustal structures) (Goldfarb et al., 1993; Goldfarb and Groves, 2015). Such polyphase deformation evolution generally leads to a complex tectonic history involving several stages of folding, overprint by late brittle deformation. Therefore, accurately determining the deformation evolution at deposit scale is crucial to identify new deposits and/or mineralized extensions. To achieve these goals, it is crucial to understand the evolution of deformation events at a deposit scale combined with the associated vein paragenesis (Perret et al., 2020; Combes et al., 2022).

In this contribution, we present new structural and geophysical datasets from one gold deposit located in the Rhyacian greenstone belts from French Guiana: the Boulanger Project (Fig. 1). We particularly emphasize the important role of polyphase deformation in the gold remobilization processes.

2. geological Background

The Guiana Shield corresponds to the northern portion of the Amazonian Craton (Delor et al., 2003). With a total area of 900,000 km^2, it covers eastern Venezuela, Guyana, Suriname, French Guiana, the northern end of Brazil and easternmost Colombia (e.g., Delor et al., 2003; Daoust et al., 2011; Tedeschi et al., 2020) (Fig. 1A). Although remnants of the Archean basement are preserved in the Amapá Block in northern Brazil and in the Imataca Complex in eastern Venezuela (Avelar et al., 2003; Tassinari et al., 2004; Barreto et al., 2013; Tedeschi et al., 2020), the Guiana Shield is mainly composed of Paleoproterozoic rocks accreted and affected by tectonics during the transamazonian orogeny at 2.2–2.0 Ga (Vanderhaeghe et al., 1998; Milesi et al., 2003; Delor et al., 2003a, 2003b). The oldest Paleoproterozoic terranes are located along the northeast margin of the Guiana Shield which corresponds to the trans-Amazonian Province (Vanderhaeghe et al., 1998; Santos et al., 2000; Tedeschi et al., 2020). In French Guiana, the trans-Amazonian Province is composed by large Rhyacian (2.20–2.05 Ga) granite-greenstone belts (northern and southern belts) which include Rhyacian volcano-sedimentary sequences, intrusive granitoids and TTG (tonalite-trondhjemite-granodiorite), and the Upper Detrital Unit that formed along the North Guiana Trough (NGT) contemporaneously to potassic granite suite (2.1–2.08 Ga) (Vanderhaeghe et al., 1998; Santos et al., 2000; Tedeschi et al. 2018, 2020; Guiraud et al., 2020). The greenstone belts are known to host multiple gold deposits (e.g., Milesi et al., 1995; Milesi et al., 2003; Guiraud et al., 2020; Combes et al., 2021).

The geodynamic evolution of the northern and southern greenstone belts of French Guiana cannot be fully elucidated due to the strong overprinting by later events (mostly D_2, from Delor et al., 2003). The evolution proposed here is largely based on structural constraints made through volcano-sedimentary greenstone belts and regionally associated plutonic rocks (see review of Delor et al., 2003 for further details). A two-step tectonic evolution has been proposed for northern French Guiana involving two major tectono-metamorphic events, D_1 and D_2, both composing the Transamazonian orogeny (Ledru et al., 1991; Vanderhaeghe et al., 1998; Delor et al., 2003). These events affected the greenstone belts and the granite-gneiss complexes (Lasserre et al., 1989; Ledru et al., 1991), whereas only the major D_2 deformation has been recognized in the Upper Detrital Unit (UDU) in northern French Guiana.

The Main Transamazonian orogeny, D_1 (ca. 2.18–2.13 Ga), is associated with magmatic accretion and crustal recycling (Vanderhaeghe et al., 1998; Delor et al., 2003). This event follows the formation of tholeithic juvenile oceanic crust exposed within the “Ile de Cayenne” complex, by the formation of calk-alkaline greenstone-TTG magmatic arcs and associated TTG (ca. 2.18–2.16 Ga) (also known as “Complexe Guyanais”). Absolute time correlations are difficult to make in the volcano-sedimentary sequences, and more accurate constraints have been established based on plutonic rock relationships. Thus, the earliest datable deformation structures are round, imbricated magmatic fabrics associated with central French Guiana calc-alkalic and TTG batholiths (ca. 2.15 to 2.13 Ga) and down-dip mineral lineations indicative of normal movement in thermal aureoles around ca. 2.13 Ga tonalites in the northern basin (Delor et al., 2001; 2003 b). These details point to the close relationship between all D_1 events (thrusting and magmatism-related deformation) and calc-alkalic and TTG plutonism.

The second deformation events, D_2, corresponds to a transcurrent tectonic event which produced E-W to NW-SE sinistral transtensional

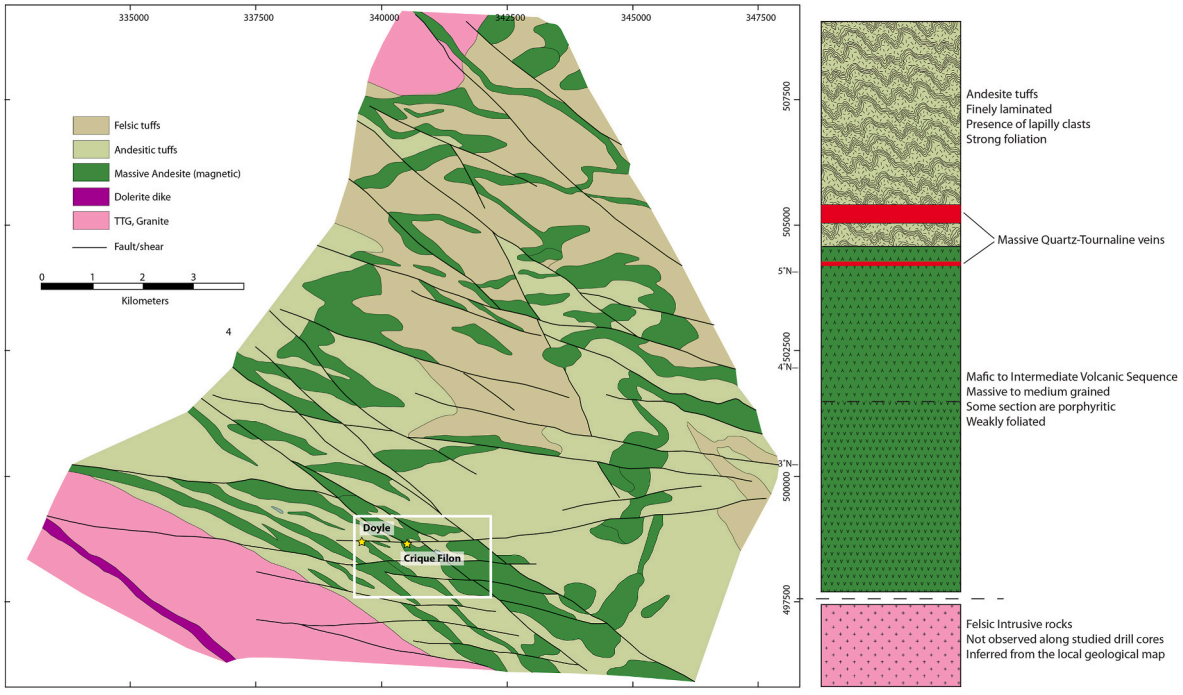

Fig. 2. Geological map of Boulanger district interpreted from airborne magnetic survey (Resources Reunion internal report) and synthetic stratigraphic column of Crique Filon area. The white rectangle corresponds to the extent of Fig. 4.

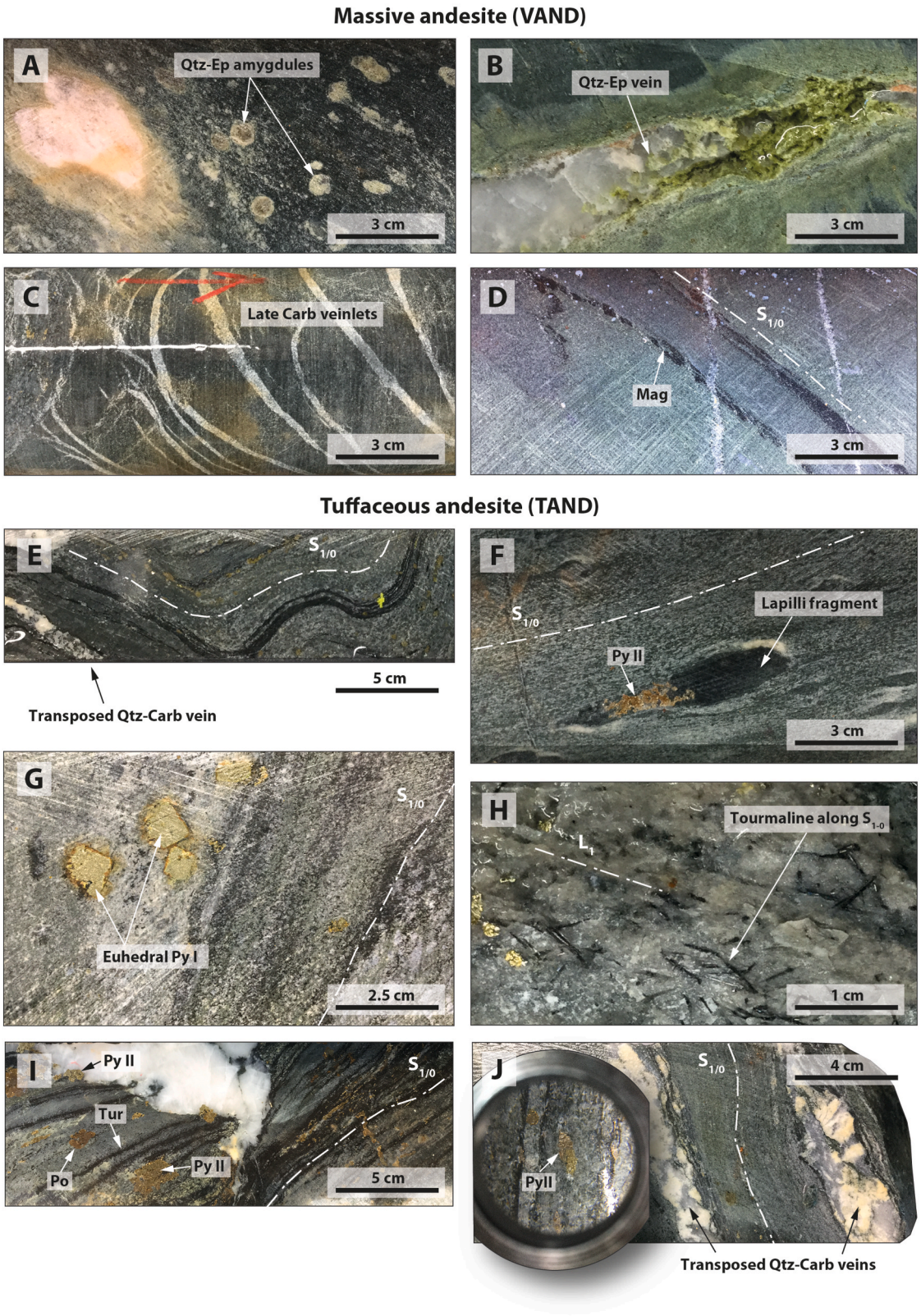

Fig. 3. Macroscopic observations of massive (VAND) and Tuffaceous (TAND) Andesite made along drill cores. **A**. Amygdules filled with quartz and epidote. **B**. Example of quartz – epidote extension vein crosscutting $S_{1/0}$ foliation. Note the epidote alteration. **C**. Classic late carbonate veinlets crosscutting massive andesite/basalt. **D**. presence of magnetite (black layers) highlighting $S_{1/0}$. Core diameter is 4.76 cm (NQ drill size). **E**. Example of folds affecting $S_{1/0}$. **F**. Fully chloritized Lapilli fragments. Note that the fragments are stretched parallel to the foliation. **G**. Euhedral mm-size pyrite crystals. D. Tourmaline parallel to the foliation. **H**. Example of D_1 quartz-tourmaline extension veins crosscutting the foliation. **I**. Example of quartz-carbonate veins transposed to the main foliation. Core diameter is 4.76 cm (NQ drill size).

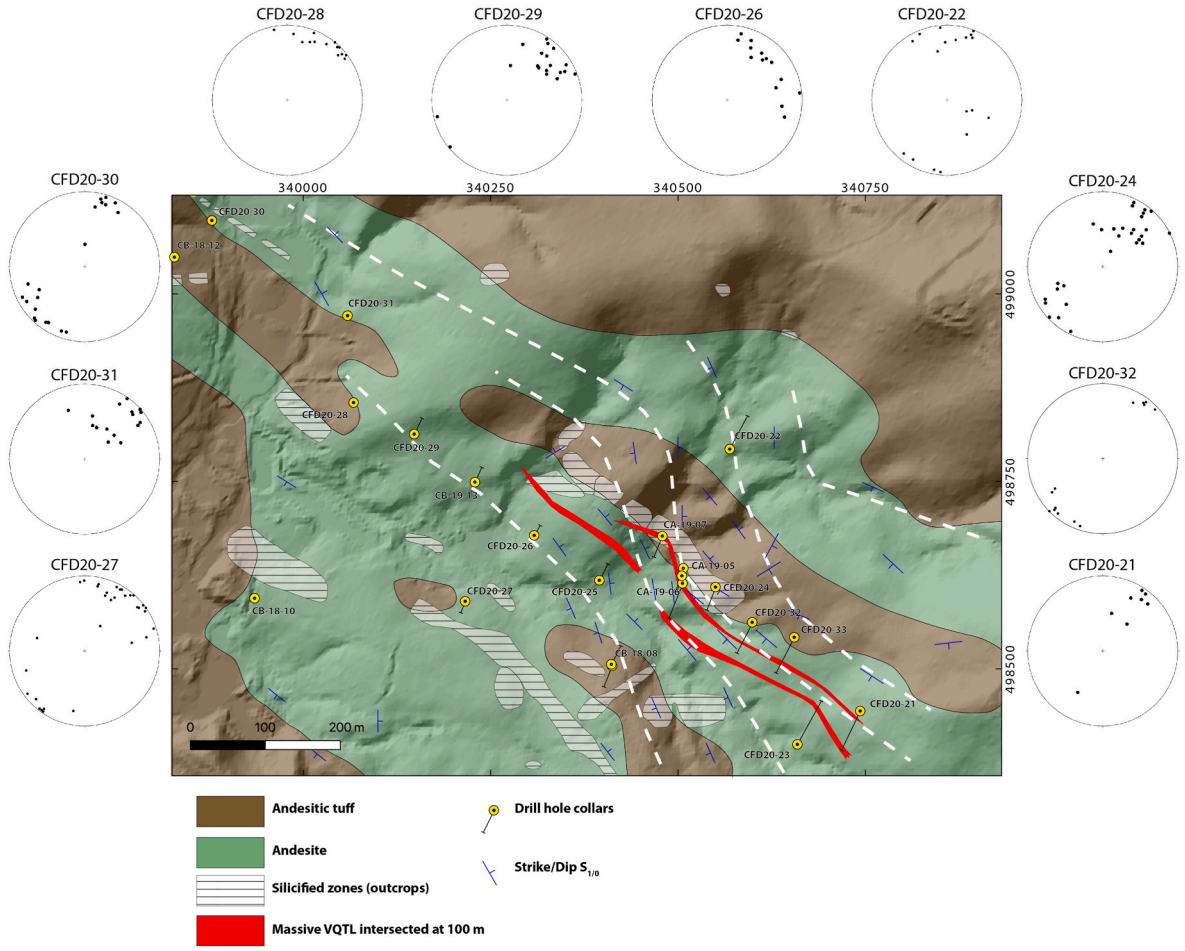

Fig. 4. Detailed geological map of Crique Filon prospect. The stereodiagrams show the distribution of the pole of $S_{1/0}$ for each drill core (Drill location on the map).

basins, mapped across French Guiana (Lasserre et al., 1989; Ledru et al., 1991; Egal et al., 1992; Milesi et al., 1995; Vanderhaeghe et al., 1998; Delor et al., 2003, 2003b) (Fig. 1A). In northern French Guiana, the D_2 event is contemporaneous to the opening of a series of "pull-apart"-type basins aligned approximately E-W and filled by conglomerate and clastic sediments which compose the Upper Detrital Unit (Ledru et al., 1991; Egal et al., 1992; 1994, 1995) (Fig. 1A).

According to Milesi et al. (1995) and Delor et al. (2003), the D_2 event is the major event responsible for gold-mineralization. The age of this deformation event is bracketed by younger granite and leucogranite with ages varying from ca. 2.1 to 2.0 Ga (Vanderhaeghe et al., 1998; Milesi et al., 2003). This granitic suite is widely documented in southern and western French Guiana (Milesi et al., 1995; Delor et al., 2003) and was emplaced during D_2.

2.1. General greenstone belt stratigraphy

The Rhyacian greenstone belts are known by different names across the Guiana Shield (Tedeschi et al., 2020). These names include the Barama-Mazaruni Supergroup in Guyana, Pastora Group in Venezuela, Marowijne Supergroup in Suriname, and the Paramaca Series in French Guiana. In French Guiana, the stratigraphy of the Paramaca Greenstone Belts has been described by Guiraud et al. (2020) and consists of.

1 A lower sequence of basalts and gabbros, interlayered with komatiitic flows (Delor et al., 2003). Locally, these mafic units are metamorphosed to amphibolites;
2 Calc-alkaline intrusive magmas and related andesitic to rhyolitic flows, and intermediate composition tuffs. The tuffaceous series is interlayered with clastic sediments and cherts;
3 A turbiditic sedimentary sequence (known as the "Armina Formation") composed of intercalated pelite, greywackes, fine sandstones and rare conglomerates interbedded with tuffs.

2.2. Mineralization

The Rhyacian greenstone belts of the Guiana Shield are preferential hosts for primary gold mineralization (e.g., Milesi et al., 2003; Delor et al., 2003; Tedeschi et al., 2020; Guiraud et al., 2020; Combes et al., 2022) (Fig. 1B). Three types of primary gold deposits have been recognized in French Guiana: 1) stratiform (VMS-type) (e.g, Dorlin, Montagne d'Or), 2) orogenic (Loulouie, Yaou, Combes et al., 2022), and 3) paleo-placer as gold-bearing conglomerates (Milesi et al., 2003). Numerous orogenic gold deposits (including the Boulanger deposit) are distributed along the North Guiana Through (NGT), an ESE-WNW trending crustal-scale shear zone located between French Guiana and Suriname within the northeastern part of the Guiana Shield (Fig. 1B).

3. Deposit geology

The Boulanger deposit consists of a series of showings including Doyle, Crique Filon and Crique Loulou belonging to the same N120-130 mineralizing trend (Fig. 2). The description below essentially concerns Crique Filon and Doyle occurrences (Fig. 2).

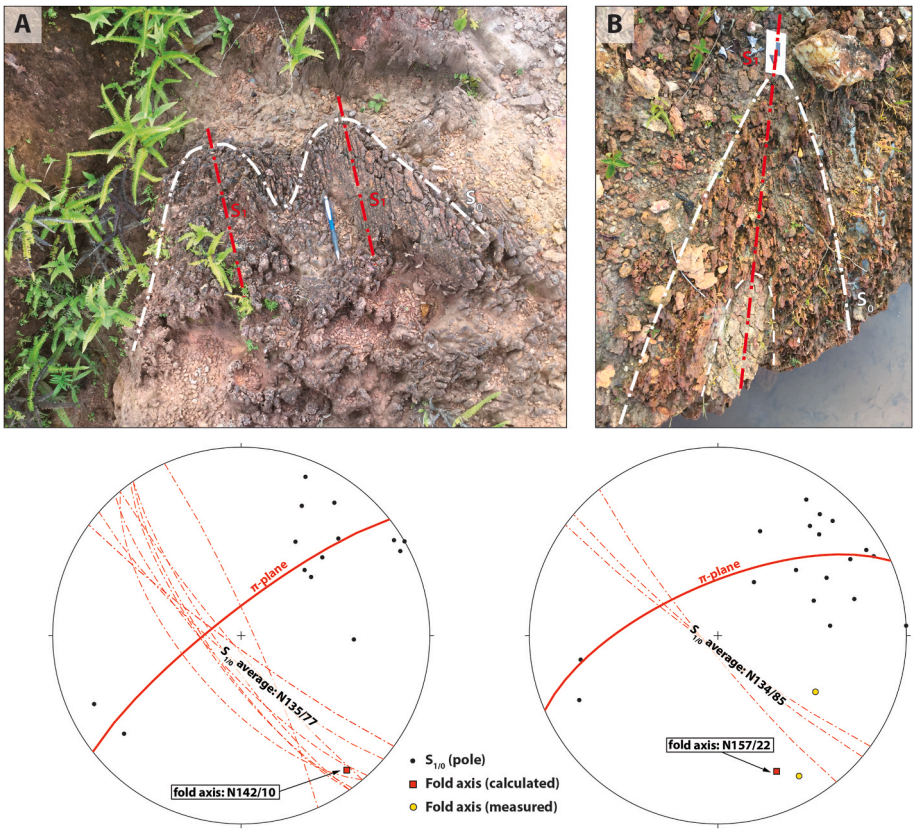

Fig. 5. Field and drill core evidence of $S_{1/0}$ folding and axial plane foliation. Note that bedding and $S_{1/0}$ are commonly sub-parallel to the bedding. Stereodiagrams. Left: structural data from A. Right: structural data from B.

3.1. Lithostratigraphy

The stratigraphy at Boulanger belongs to the Paramaca Series, a Paleoproterozoic volcano-sedimentary series dominated by mafic to intermediate compositions (Vanderhaeghe et al., 1998; Delor et al., 2003). Locally, the mineralization (defined by massive quartz-tourmaline ± pyrite veins; see sections 3.2.2) is hosted by massive andesite (VAND) and/or Andesitic tuffs (TAND) (Fig. 3). The descriptions proposed below are based on macroscopic observations.

3.1.1. Massive andesite (VAND)

VAND correspond to aphanitic to microcrystalline massive greenish volcanic rock which could locally present evidence of amygdales (Fig. 3A). VAND are crosscut by abundant mm—to cm-thick quartz-calcite and quartz-carbonate-chlorite veins (Fig. 3B and C). Quartz-rich veins are generally associated with an epidote alteration halo (Fig. 3C). The amygdales are generally filled by quartz-pyrite assemblage with also common epidote alteration (Fig. 3A). Sulfide and oxide minerals are present and correspond to disseminated magnetite, pyrite and locally pyrrhotite (Fig. 3D).

3.1.2. Andesitic tuffs (TAND)

Andesitic tuffs (TAND) are heterogeneous in terms of texture, grain sizes and mineral contents. Our current petrographic observations are based on available drill cores, and therefore do not allow to fully assert the lateral facies variation of tuffaceous series in great details. Andesitic tuffs usually show millimetric to centimetric laminations, with variable amounts of tourmaline, sericite, chlorite, quartz and carbonate (Fig. 3 E, F, G). A foliation parallel to the bedding, referred as $S_{1/0}$, is present (Figure E, G). Andesite tuffs are commonly associated with the presence of euhedral pyrite (Py I), developed within the microcrystalline matrix, and tourmaline along the foliation (Fig. 3G–I). Pyrite crystals (Py I) commonly show the presence of pressure shadow parallel to $S_{1/0}$ suggesting they formed prior or during $S_{1/0}$ foliation. $S_{1/0}$ foliation features a L1 pyrite-bearing mineral lineation that plunges 65° toward the N085 (Fig. 3 H). Locally, TAND contain mm-to cm-sized mafic chloritized lapilli fragments (Fig. 3F). Lapilli fragments are stretched parallel to $S_{1/0}$ foliation and record strain varying from 1 to up to 7. Lapilli fragments can be affected by boudinage with interboudin domains filled by secondary pyrite (Py II) (Fig. 3F), suggesting that pyrite is also synkinematic. Whereas pyrite is the dominant sulfide minerals, disseminated pyrrhotite parallel to sub-parallel to the foliation has been locally described (Fig. 3J). Numerous quartz-carbonate-tourmaline veins have been observed within TAND (Fig. 3E–I, J). They are either transposed to the main foliation, featuring pinch-and-swell texture (Fig. 3E–J), or crosscut the foliation (Fig. 3I).

3.2. field and structural observations

Detailed structural analyses have been conducted on both outcrops and along oriented drill cores from the 2020 drilling campaigns done by Reunion Gold Corporation (Crique Filon target: CFD20-21, CFD20-22, CFD20-24, CFD20-25, CFD20-26, CFD20-27, CFD20-30, CFD20-31, CFD20-32, CFD20-33; Fig. 4). In total, three deformation stages have been defined.

3.2.1. coaxial folding and quartz-tourmaline vein emplacement

3.2.1.1. $S_{1/0}$ foliation. Although intensively weathered, evidence of bedding (S_0) affected by tight to isoclinal folds has been observed within tuffaceous rocks at surface and along drill cores (Fig. 5). The overall stratigraphic series is affected by a pervasive regional axial planar foliation, referred as $S_{1/0}$, parallel to sub-parallel to the bedding (Fig. 3D, E, G and Fig. 6A). At regional scale, $S_{1/0}$ orientation is homogeneous,

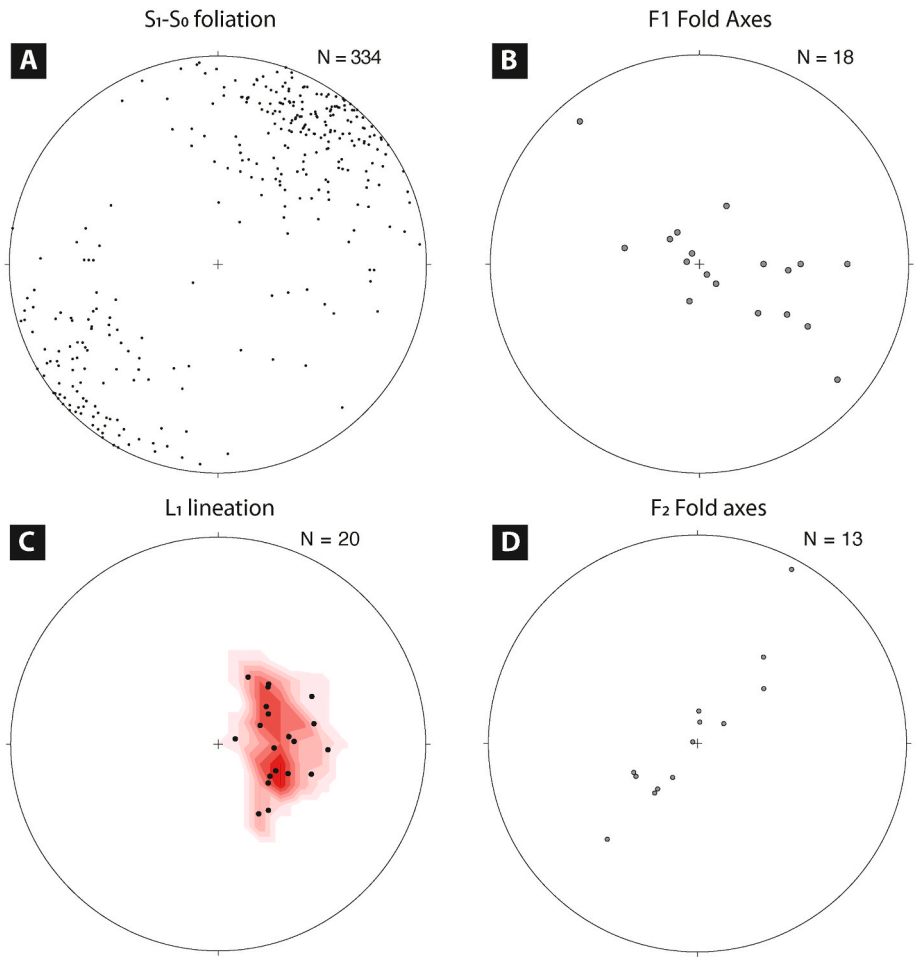

Fig. 6. Stereodiagrams (equal area, lower hemisphere) showing the different structures measured along drill cores. A. Pole of S1/0. B. Measured fold axes. C. Measured mineral lineation (tourmaline, pyrite, sericite). D. F2 fold axes determined by structural analysis.

mainly oriented N120-N140 (Fig. 6A), consistent with regional tectonic grain (Delor et al., 2003; Vanderhaeghe et al., 1998). The distribution of foliation poles support that $S_{1/0}$ is affected by tight folds oriented N120-140 (Figs. 5 and 6A). $S_{1/0}$ foliation features tourmaline, pyrite or sericite stretching lineation (l_1), which is plunging of about 65° to N088 (Fig. 3H; Fig. 6C). Occasionally, some crosscutting relationship between $S_{1/0}$ (axial plane foliation) and the bedding are visible along fold hinges (Fig. 5). Most of $S_{1/0}$ foliation is pseudo-parallel to the fold axial planes, suggesting both structures are contemporaneous and likely formed in response to a NE-SW compressive event (D_1). Although measured fold axes generally follow the regional N130 trend, their plunging directions vary from SE to NW (Fig. 6B), suggesting the presence of polyphase deformation.

3.2.1.2. Quartz tourmaline veins (VQTL). Quartz tourmaline vein (VQTL) system which composes to the main exploration target, is defined by a set of extension and shear veins (Fig. 7A and B; Fig. 8).

Shear veins consist of massive (thickness varying from 20 cm to > 12 m) tabular bodies oriented N120 and dipping 75° toward the south (Fig. 7A and B, Fig. 8A) and developed along shear zones. Shear veins are laminated and generally contain inclusion trails, rhombus shape quartz, suggesting the opening by oblique crack-seal texture (Labaume et al., 1991; Lacroix et al., 2020; Bons et al., 2012). Locally, shear veins are crosscut by dilatational jogs where brecciated Tourmaline-rich material can be observed (Fig. 8B). Proximal alteration of massive shear veins consists to meter-wide intense tourmaline alteration (almost 100% tourmaline), whereas the more distal altered host rock consists to tourmaline-rich mafic tuffs, is associated with the mm-to cm-wide tourmaline ± calcite replacement zones parallel to $S_{1/0}$. These shear veins can reach several hundred meters of lateral extension (Fig. 4). The N120-140 orientation of quartz-tourmaline veins also agrees with the trend defined by mapping based on the distribution of quartz boulders and silicified zones (Fig. 4).

Extension veins consist of sub-horizontal cm-to dm-thick planar bodies striking at about N320 and dipping about 10° toward NE (Fig. 7C). Extension veins are commonly filled with interdigitated quartz and tourmaline minerals perpendicular to the contact with host rock supporting a Mode I opening and mineral crystallization from the host-rock toward vein center (Fig. 8C) (Bons et al., 2012). Pyrite and chalcopyrite are also present, generally along the outer part in contact with the host rock (Fig. 3I). Quartz - tourmaline extension veins are associated with a sericite-tourmaline alteration of the proximal host rock (Fig. 3H).

Along drill cores, extension and shear veins do not show clear crosscutting relationship. However, several observations suggest that they are rather connected. Kinematic indicators of shear veins, such as slickenslide, striation, and the angular relationship with contemporaneous extension veins and foliation suggest that they formed along reverse shear/faults in response of a NE-SW compressive stress (D_1) (Fig. 7D).

The geometry of both extension and shear veins gives an opportunity to determine the stress field orientation during deformation (e.g.,

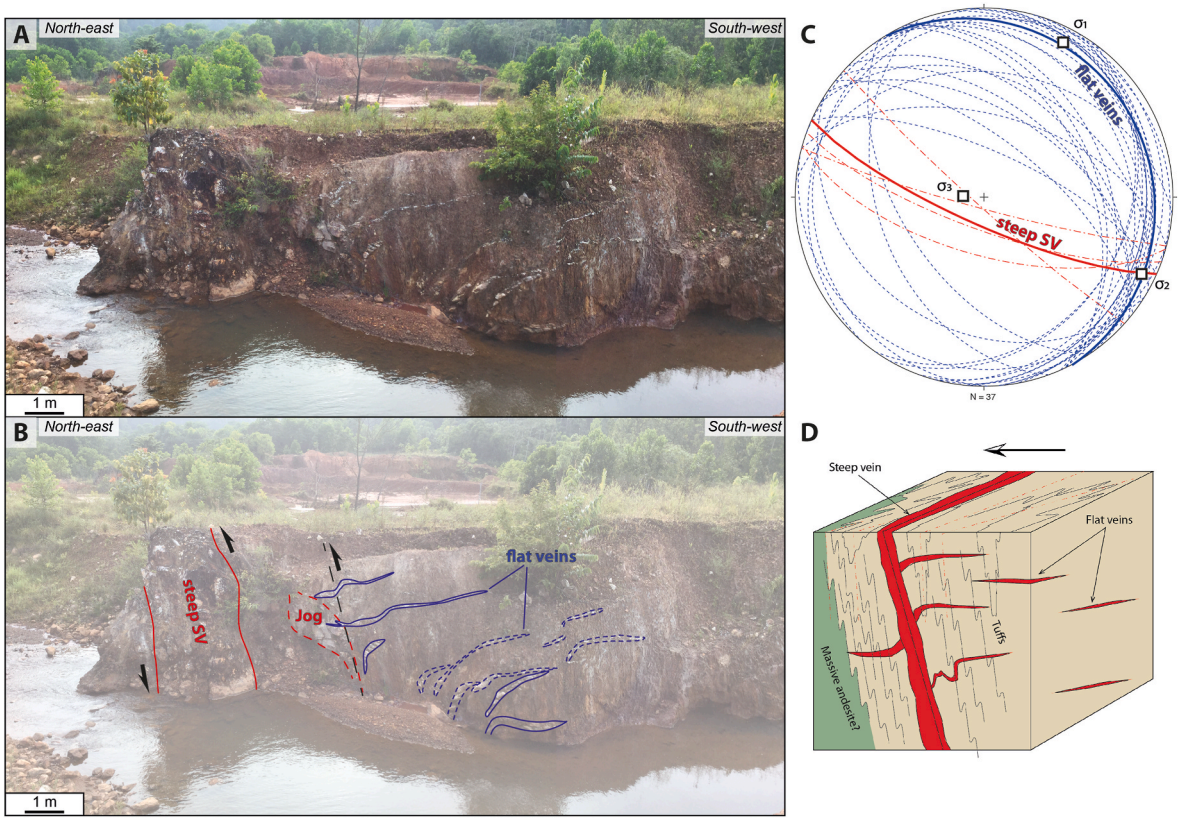

Fig. 7. Example of D_1 quartz-tourmaline vein system observed within Boulanger prospect. **A** and **B**. Field picture and interpretation showing the geometry of D_1 mineralized system. Note the presence of sub-horizontal (flat; blue) veins connected to steeply southwest dipping massive shear vein (red). **C**. stereographic projection of both shear (red) and extension (blue) veins. **D**. Block diagram showing the geometry of the D_1-mineralized system.

Sibson, 2020). Extension veins form perpendicular to the minimum principal stress (σ_3) and along the σ_1-σ_2 plane (e.g., Bons et al., 2012; Van Noten et al., 2011; Lacroix et al., 2013). In contrast, shear veins form oblique to both the maximum and minimum principal stresses, σ_1-σ_3 (Fagereng et al., 2010; Bons et al., 2012; Sibson, 2020) with σ_2 given by the intersection between EV and SV. Using this spatial relationship, the paleo-stress field is characterized by a sub-vertical minimum principal stress, and sub-horizontal maximum principal stress, σ_1, oriented N026 (Fig. 7C).

3.2.2. *Evidence of a second deformation event*

Within Crique Filon area, both $S_{1/0}$ foliation measured in the field and along cores are locally re-oriented along a NS trend (Fig. 4). A similar statement can also be made by quartz – tourmaline massive veins intersected by drill cores (red polygons on Fig. 4; note that they correspond to surface projection of the mineralized system intersected at 100 m depth). Such structural reorientation suggests the presence of another deformation event.

In order to better constrain this second event, we used $S_{1/0}$ foliation dataset from surface and from ten oriented DDHs from the 2020 drilling campaigns within the Crique Filon target (CFD20-21, CFD20-22, CFD20-24, CFD20-25, CFD20-26, CFD20-27, CFD20-30, CFD20-31, CFD20-32, CFD20-33) to determine the axial surface orientation of the shear event D_2 (F_2) (Fig. 9). The distribution of $S_{1/0}$ foliation defines a series of several distribution planes (π-planes) (Fig. 9). All the calculated fold axes share the same N030-040 axial surface (Fig. 6D). Note that the distribution of poles of foliation agree with type-1 fold interference pattern (e.g., Ramsay, 1967) (Fig. 9). In such polyphase folding context, F_1 fold limbs ($S_{1/0}$) are affected by steeply plunging F_2 folds with the fold plunge and plunging direction both controlled by the pre-D_2 dip angle of $S_{1/0}$ foliation.

D_2 deformation is not pervasive and only observed along narrow domains oriented N040 that seem spatially correlated to the drainage system such as Crique Filon.

3.2.3. *D_3-late brittle deformation*

Late deformation event observed within the studied area (D_3) is marked by the development of conjugated brittle fault surfaces oriented N085/55 and N260/40, respectively (Fig. 10). The fault surface can feature striations plunging at about 20° toward N110, in agreement with an important strike-slip component (Fig. 10). Because these late structures are not associated with gold mineralization and do not play a significant role on the mineralization shifting, they will not be discussed further.

4. mineralization

The Au mineralization at the Crique Filon prospect is complex and records a polyphase or progressive deformation history. In order to better understand the relationship between deformation and mineralization events, we discuss the mineralization as D_1-and D_2-related mineralization. Note that this description is based on macroscopic observations only.

4.1. *D_1 mineralization*

Volumetrically, the most significant mineralized structures consist of extension and shear vein system predominantly composed of quartz and tourmaline (Tur I) with minor amount of carbonate and pyrite (Py II) ± chalcopyrite (Fig. 11A; Fig. 12), as well as the adjacent altered host rock (Fig. 8). Along drill cores, the quartz-tourmaline vein thickness varies from 1 cm to up to 11 m (Fig. 8A), with gold grade generally below 2 g/

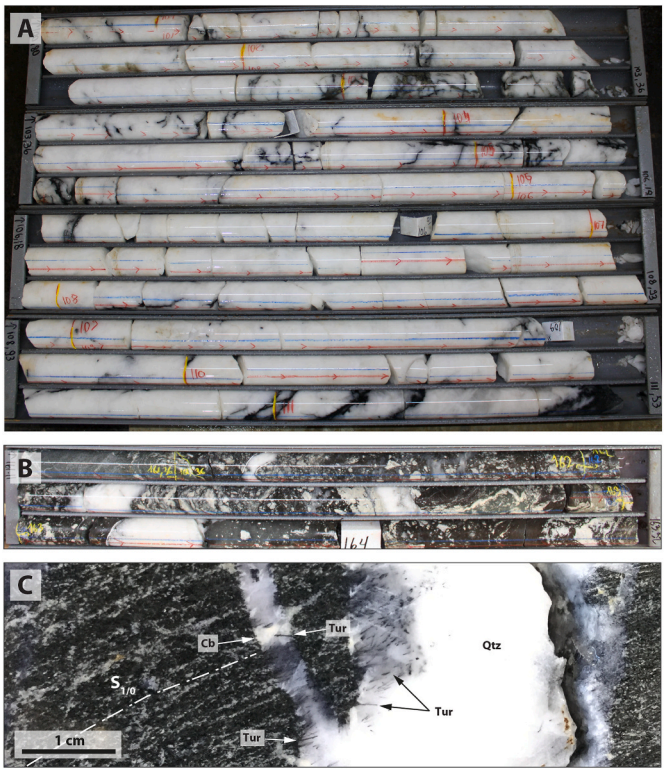

Fig. 8. Example of quartz – tourmaline vein system intersected along drill core. A. Massive (>1 m thick) shear vein (Drill hole CF20-25, 100.8–111.53 m depth interval). B. Detail of brecciated VQTL filled by tourmaline-reach matrix (Drill hole CF20-21 at 162 m depth). C. Quartz-tourmaline extension vein. Core diameter is 4.76 cm (NQ drill size).

ton. The mineralized envelope is defined by a hydrothermal alteration of the direct host rocks marked by the assemblage tourmaline – sericite – pyrite (Fig. 3I and 11A). The intensity of tourmaline alteration could vary from partial, with the development of tourmaline-rich foliation with tuffaceous rocks adjacent small veins, to pervasive forming massive tourmaline bodies within the direct host rock adjacent to massive shear veins.

4.2. D_2 mineralization

Macroscopic observations made along the highest-grade drill intersections systematically show the presence of pyrrhotite-pyrite ore assemblage (Fig. 12), along with the presence of visible gold along late fractures affecting D_1 quartz-tourmaline veins (Fig. 11 B, C, D). Within these depth-intervals, pyrrhotite is either disseminated along the foliation, forming mm-scale grains parallel to $S_{1\text{-}0}$ foliation (Fig. 11C and D), or more massive and abundant along $S_{1\text{-}0}$ fold hinges, suggesting space opening by foliation delamination (Fig. 11 C). Because this mineralization stage is not pervasive, e.g., associated with the pervasive fluid flow through the porous media, no important alteration front is documented. These new observations suggest that the highest gold grades are not macroscopically associated with the same ore assemblage and structures as for D_1-mineralization (Fig. 8). We suggest that this new ore assemblage corresponds to a second mineralization/deformation stage (Fig. 12). Indeed, highest gold grades are almost systematically associated to the presence of pyrrhotite and D_1-quartz veins fractures (Fig. 11B), and/or small bodies formed by the delamination of $S_{1/0}$ foliation (Fig. 11C and D) in response to structural reorientation. Some evidence of visible gold along fractures developed within quartz veins have also been reported along DDH CFD20-25, which once again, supports a late mineralization event. Interestingly, the zone affected by D_2

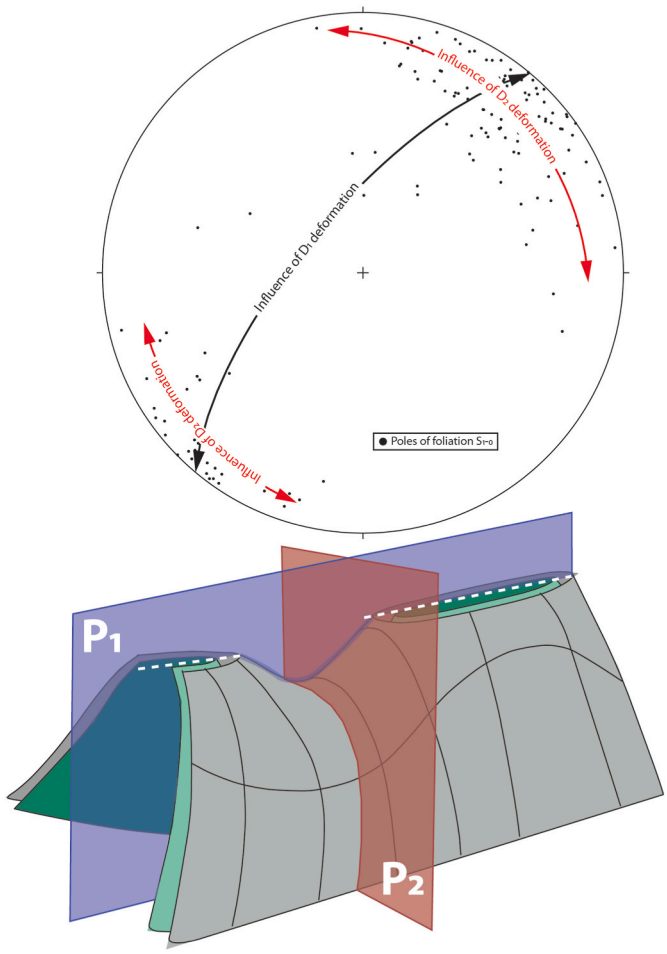

Fig. 9. Conceptual block diagram showing the re-orientation of D_1 structures and mineralized system along N020-030 D_2 corridor. The stereodiagram (equal area, lower hemisphere) shows the distribution of the poles of $S_{1/0}$ foliation measured along drill core from Crique Filon area.

reorientation (e.g., Crique Filon; Fig. 4) and exhibit the best Au-grade (3 m at 22.3 g/t). These zones are characterized by higher Au-grade, and the presence of pyrite and cm-thick bodies of pyrrhotite (Fig. 11C and D). Note that these latter features are not present (or at least at macroscopic scale) within D_1 mineralization.

5. Geophysical interpretation

Due to the deeply weathered profile, which is typical from humid and tropical region, surface geological information is sparce and almost exclusively relies on drill cores (e.g., Combes et al., 2022). To increase knowledge on the geology and structures at property scale, the fabrics documented on the field and along drillcores at micro- and macro-scales are integrated to the regional Airborne and Ground geophysical data in order to propose the tectonic framework of the Boulanger district. Regional-scale interpretation of the French Geological Survey airborne radiometric and magnetic have been already proposed by Delor et al. (2003). However, the regional-scale of investigation did not allow to resolve geophysical heterogeneity at the Boulanger deposit-scale.

5.1. Lithological distribution

At deposit scale (e.g., Crique Filon site), the distribution of the main stratigraphic units is well defined from surface geological mapping, trenching and drill core data (Fig. 4). The induced polarization map presented in Fig. 13B highlights zones with differences in the subsurface

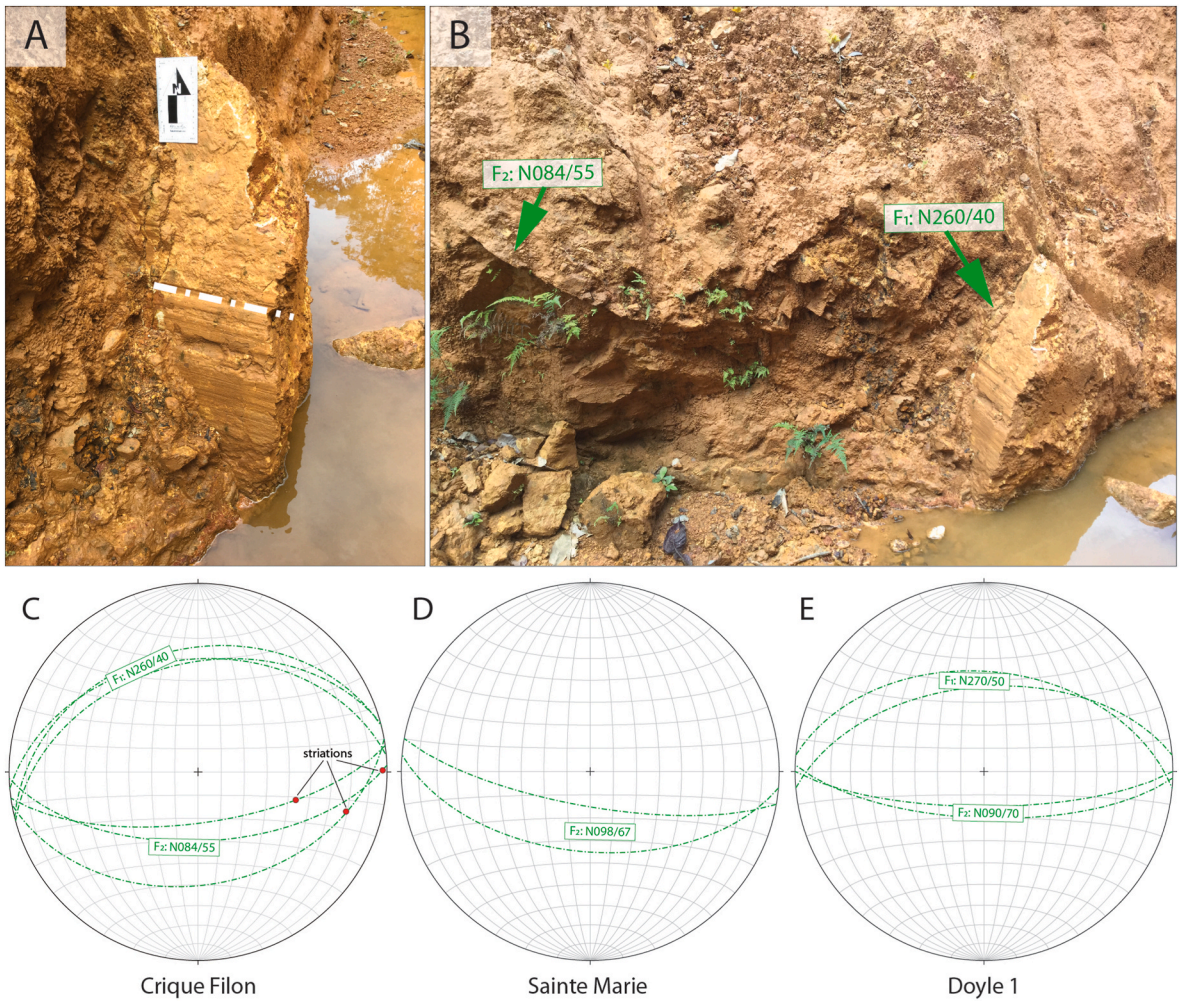

Fig. 10. Example of D3 brittle structures observed on surface. Note that most of the measured striations indicate a strike-slip movement (stereodiagrams are equal area, lower hemisphere).

chargeability. Induced polarization (IP) is largely used for mapping ore bodies and host rocks that are associated with disseminated sulfides and massive sulfide bodies (Sumner, 2012; Gurin et al., 2018). Based on our drill core description and mapping, the higher chargeability stratigraphic units may be spatially correlated with the andesitic tuffs (TAND), as they contain important euhedral primary pyrite (Fig. 3G). In contrast, the low chargeability areas correspond to the mafic volcanic rocks (VAND). Note that both low- and high-chargeability units define folded patterns oriented N120-130 parallel to D_1 structures (e.g., $S_{1/0}$, F_1 fold axes). Interestingly, the main known quartz-tourmaline mineralization intersected along diamond drill holes and documented at surface (Fig. 4) are located along the sharp contacts between the two contrasted chargeability surfaces (Fig. 13B). These observations suggest that the contact between andesite and tuffaceous rocks localizes the mineralization, supporting our observations along drill cores.

Similar observations can be made from the Total Magnetic Intensity grid (TMI) (Fig. 13A). The high magnetic zones are associated with mafic to intermediate massive volcanic rocks (VAND) from the Paramaca series. Indeed, this is supported by the presence of disseminated magnetite (Adagunodo et al., 2015) within massive andesite (Fig. 3D), magnetite being known as one of the few minerals responsible for significant magnetic anomalies (Adagunodo et al., 2015). In contrast, the low magnetic area highlights the tuffaceous andesite. TMI data also highlight the contact between the Paramaca volcaniclastic series and the granodiorite to the south, as well as the presence of a strong magnetic NW-SE lineament which corresponds to a regional dolerite (Delor et al., 2003) (Fig. 13A).

5.2. *Identified structures*

Both airborne Magnetic and ground Induced polarization data are used to delineate the main structures at property scale. Both the IP and magnetic maps highlight clear evidence of type-1 fold interference patterns (e.g., Ramsay, 1967) (Fig. 13A and B). The presence of such fold geometry is also supported by the distribution of $S_{1/0}$ (Fig. 9) and fold axes (Fig. 6B) both measured on surface and along drill cores. Such fold interference pattern is likely to be produced by polyphase folding involving the superposition of F_1 fold axial surface oriented N120, and N020 trending upright F_2 fold axial surface.

The observations from the Total Magnetic Intensity grid (TMI) (Fig. 13A) emphasize (1) the contact between the Paramaca series and the granodiorite, (2) the presence of a N130 striking dolerite dike, (3) the lithological magnetic variation among the Paramaca series, and (4) the type-1 fold geometry affecting the Paramaca series (Fig. 13A). The TMI map also shows the presence of a low magnetic lineaments oriented N020-030. Interestingly, this lineament is spatially correlated to the Crique Yaoni stream (oriented N030) which composed the main target for current alluvial gold production (Jebrak et al., 2021).

The main results of geophysical data interpretation include: (1) the presence of N110-120 fold structures which allow the replication of the Paramaca volcanoclatsic series, (2) the presence of Type-1 fold interference patterns and their related N020 F2 axial surface (Fig. 13).

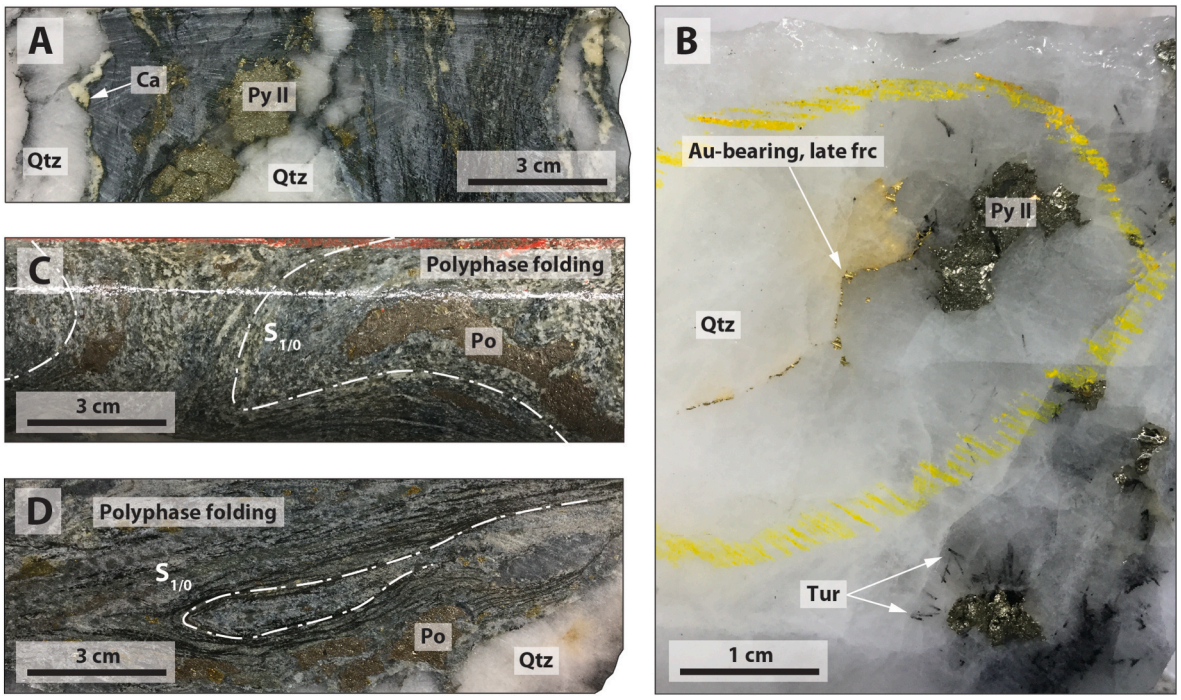

Fig. 11. Example of D_2 mineralization overprinting D_1 structures. A. D_1 mineralization associated with quartz, pyrite and carbonate, intersected by drill hole along the structural re-orientation of Crique Filon (DDH # CFD20-25, Fig. 4). Note that the mineralized structure is affected by pinch-and-swell suggesting structural overprint. B. Presence of visible gold along late fracture affecting massive D_1 VQTL (DDH # CFD20-24, Fig. 9). C and D. Example of polyphase folding developed within $S_{1/0}$ (DDH # CFD20-24, Fig. 9). Note the presence of pyrrhotite along the fold hinge. Scale bars: ~2.5 cm.

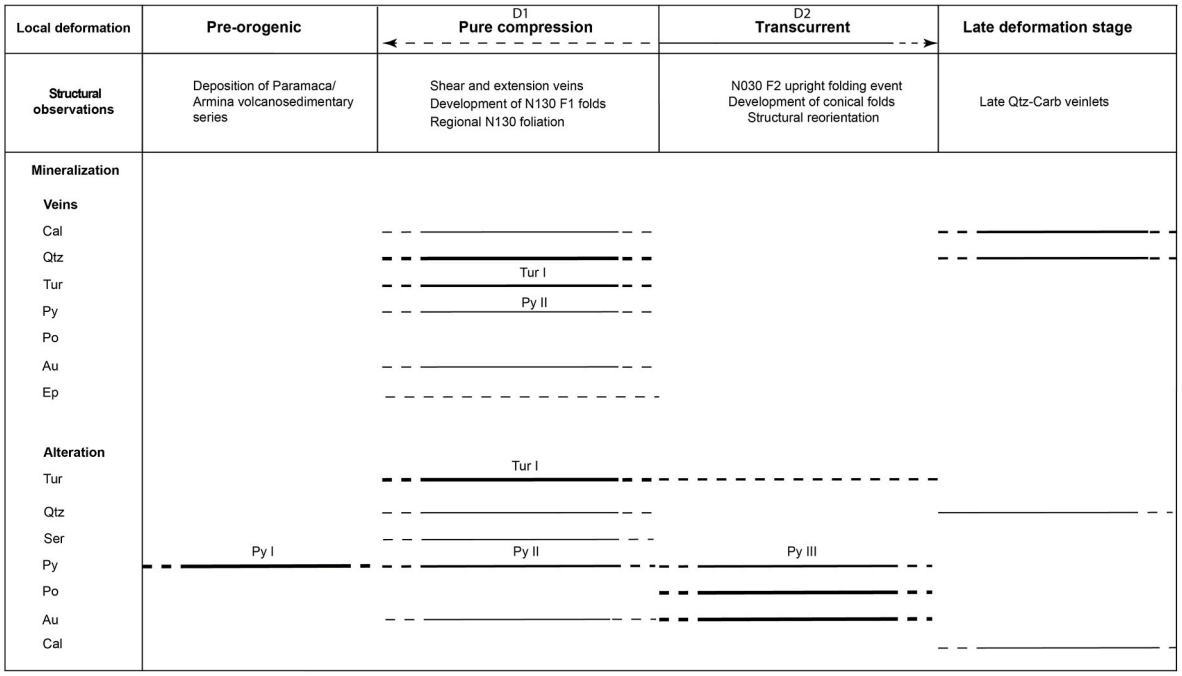

Fig. 12. Paragenetic sequence of the Boulanger Gold deposit with emphasis on deformation events.

6. Discussions

6.1. From deposit scale to regional-scale structural evolution of the Boulanger district

The structural evolution proposed below is based on an integration of regional and deposit-scale field data including airborne magnetic, Induced Polarization and structural analyses completed by Reunion Gold Corp.

Our dataset clearly illustrates that the studied area is affected by polyphase deformation invoking at least two stages of deformation/ folding, D_1 and D_2. This is especially well documented by the local reorientation of $S_{1/0}$ at Crique Filon (e.g., Fig. 4) and the type-1 fold superposition pattern highlighted by geophysical data (Fig. 13).

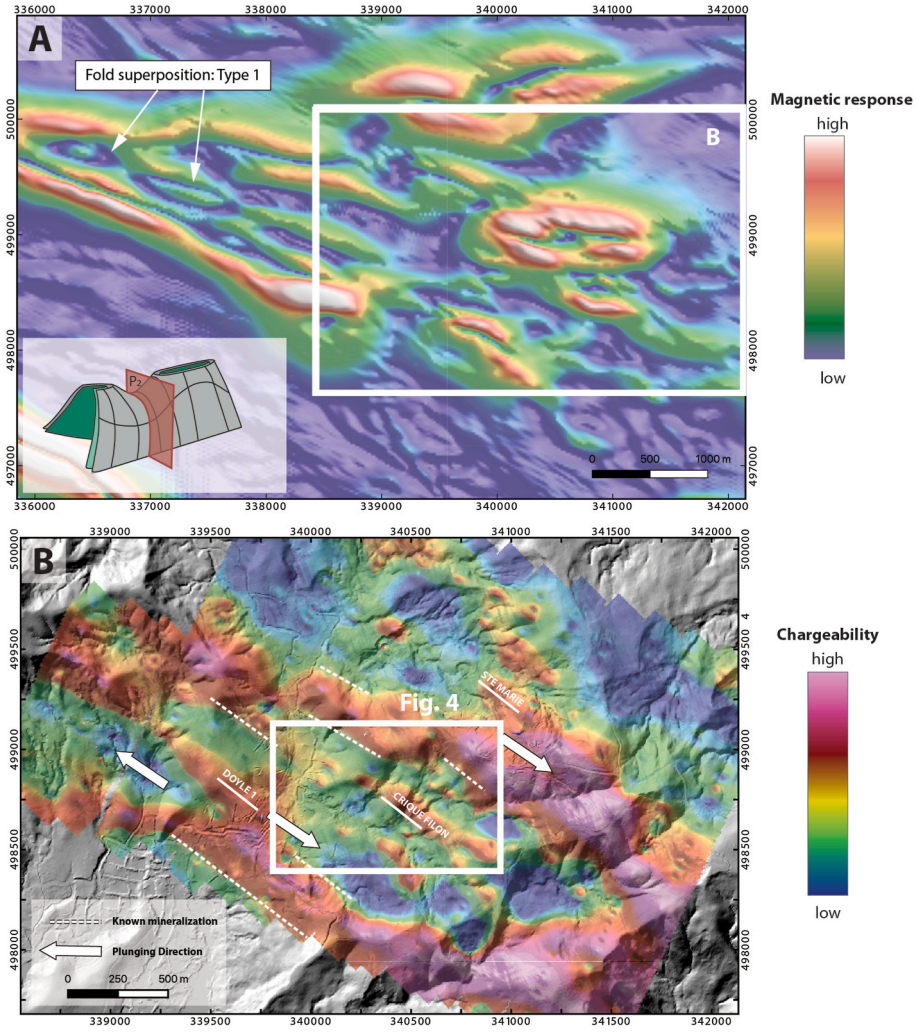

Fig. 13. A. Total Magnetic Intensity grid (TMI) map. B. Chargeability map derived from ground Induced Polarization survey.

Historically, fold interference patterns as portrayed by Ramsay (1967) would have been described as the consequence of two successive deformation phases (Ramsay, 1967; Fossen et al., 2019). However, as discussed by Fossen et al. (2019), we suggest that this fold interference pattern developed during progressive deformation involving two sub-phases, D_1 and D_2, described below.

6.1.1. D_1: pure compressional event

Deformation event D_1 is principally associated with the development of tight to isoclinal folds and a crenulation foliation $S_{1/0}$ within the volcanoclastic Paramaca Series (e.g., Fig. 5). The structural analysis made on $S_{1/0}$ suggests that the fold axes and axial surfaces are both oriented N130-150, consistent with the regional structural grains highlighted by both airborne and ground geophysical surveys (see section 5). $S_{1/0}$ is homogeneous, with an average of N135/80 (Fig. 6A), pseudo-parallel to the fold axial surfaces suggesting that both structures formed contemporaneously in response to a NE-SW shortening (Fig. 14A). This NE-SW shortening event also produced important bedding-parallel shear along fold limbs, and at contact between the two rheologically contrasted tuffaceous and massive andesites, which allow the emplacement of quartz-tourmaline-pyrite-carbonate shear and extension mineralized vein system (Figs. 7 and 8). Stress inversion performed on the mineralized system also suggests a NNE-SSW maximum horizontal stress (Fig. 7C), in line with both regional NW-trending fold and foliation. These findings agree with the geodynamical model of the Guiana Shield proposed by Delor et al. (2003) which defines a first shortening event (D1) oriented NS.

6.1.2. D_2: transcurrent deformation

Numerous evidence of transcurrent deformation are present at property scale. Whereas the exact kinematic of transcurrent deformation remains questionable, dextral evidence such as asymmetric shear folds affecting early veins are predominant. In addition, D_2 transcurrent event is marked by the systematic change in plunge and plunge direction of the F_1 fold axes (Type-1 fold superposition; Fig. 6B, 9 and 13). Indeed, measured fold axes are either plunging toward N130 or N300 (Fig. 6B), suggesting the F_1 fold system developed within volcanoclastic rocks is affected by a second stage of folding producing Type-1 interference pattern (e.g., Ramsay, 1967). We interpret that this polyphase folding results from a dextral transcurrent deformation event, D_2, in line with the geodynamical proposed by Delor et al. (2003).

In the case of Boulanger, we interpret that the property scale Type-1 interference pattern (e.g., Ramsay, 1967) results from the transition from compressional to transcurrent deformation (Fig. 14B). Indeed, complex fold interference patterns can form along shear zones where strain is partitioned between pure shear (D_1) and simple shear dominated domains (Clegg and Holdsworth, 2005; Fossen et al., 2019). The style of interference pattern recognized at Boulanger deposit, slightly differs from the type-2 fold geometry documented by Vanderhaeghe et al. (1998) in the Upper Detrital Unit exposed at Montagne Tortue located at 25 km southwest from the studied area. Similar transition to a transcurrent regime has been proposed elsewhere in the Guiana shield

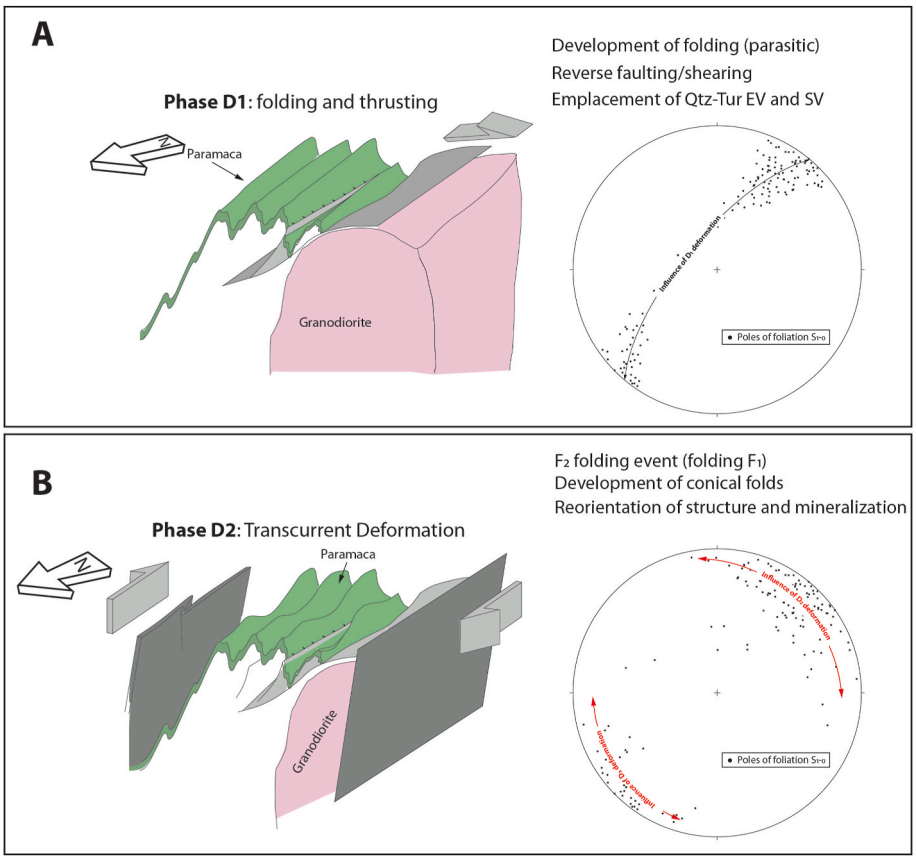

Fig. 14. Conceptual tectonic evolution model of southern Boulanger.

(French Guiana, Suriname and Guyana) by Vanderhaeghe et al. (1998), Delor et al., (2003) and Tedeschi et al. (2018).

A geodynamic evolution of the Guiana shield has been proposed by Vanderhaegue et al. (1998) and further discussed by Delor et al. (2003). At regional scale, D_1 is responsible for the main structural fabric observed along the entire North Guiana Trough (Delor et al., 2003; Vanderhaeghe et al., 1998; Daoust et al., 2011) located in French Guiana and Suriname (referred as D_1 in Delor et al., 2001). Although, the timing of D_1 deformation event and related mineralization is not constrained yet, Vanderhaeghe et al. (1998) have performed radiochronology on small syntectonic granitic plutons from Maripa area, located at 35 km SW from Boulanger. Based on their results, they propose convergence and oblique-convergence between 2093 Ma and 2083 Ma.

6.2. GOLD concentration during trancurrent deformation

As described above, it is clear that Au mineralization is associated with the development of quartz-tourmaline extension and shear vein system during D_1 compressive event (ground preparation). However, our detailed observations along drill cores suggest the development of a late pyrrhotite-pyrite assemblage along small scale F_2 fold hinges (affecting $S_{1/0}$) as well as the deposition of visible gold along fractures affecting massive VQTL (Fig. 11B), suggesting that this mineralization postdates the quartz-tourmaline vein system (shear and extension veins). We infer that this second ore stage is contemporaneous to D_2 folding event during transcurrent deformation event (see section above).

To illustrate the gold endowment related to polyphase folding, we have produced an Au grade discretization of $S_{1/0}$ foliation as function of Au grade (Fig. 15). For this, each drill interval on which foliation has been measured, has been plotted as a function to the corresponding Au results (Au assay every meter). For low grade (e.g., Au g/t varying from 0.05 to 0.1 g/t), $S_{1/0}$ foliation depicts D_1 fold trend (Fig. 15). For gold grade varying between 0.1 and 0.5 g/t, the foliation seems to be influenced by both D_1 and D_2 (Fig. 15). Finally, $S_{1/0}$ foliation from the highest gold grade intervals (>0.5 g/t) clearly display F_2 fold interference (Fig. 15). The different calculated fold axes (given by the different π-planes) are aligned along a N030 trend, which is consistent with 1) F_2 axial plane estimated from $S_{1/0}$ foliation (see section 4.3), and 2) the low magnetic N020 trend highlighted by airborne geophysical data (Fig. 13A). The results from this structural analysis demonstrate that the D_1 events is associated with low-to medium-Au grades (up to 0.5 g/t Au) (Fig. 15).

The Boulanger deposit show many similitudes with the Clearwater deposits, located in the Eastmain greenstone belt from James Bay area (Canada) (Lacroix et al., under review). Similarly, the mineralization at Clearwater is polyphase and associated with a two-fold mineralization process. The first stage of mineralization is associated with the development of a quartz-tourmaline vein system similar to Boulanger in response to a North-South shortening event (D_1) at the transition between greenschist and Amphibolite metamorphic conditions (Lacroix et al., under review). This shortening event is, then, followed by the transcurrent reactivation of crustal structures, locally producing a crenulation foliation S_2, the formation of type-2 fold interference pattern, as well as the delamination of the initial $S_{1/0}$ foliation which allows the opening of spaces filled by pyrite-pyrrhotite assemblage (similar to Boulanger deposit).

Similar gold endowment involving late transcurrent deformation have been documented in different Precambrian hosted-greenstone (De Ronde and de Wit, 1994; Jones and Kisters, 2022) and Mesozoic-Cenozoic Au-deposits (e.g., Goldfarb et al., 1993; Goldfarb et al., 2008; Goldfarb and Groves, 2015; Lacroix et al., 2020), suggesting that the transition from collisional compressive regime to transcurrent deformation is an important mechanism in the formation and maturation of orogenic gold systems (Goldfarb et al., 2008). This is particularly

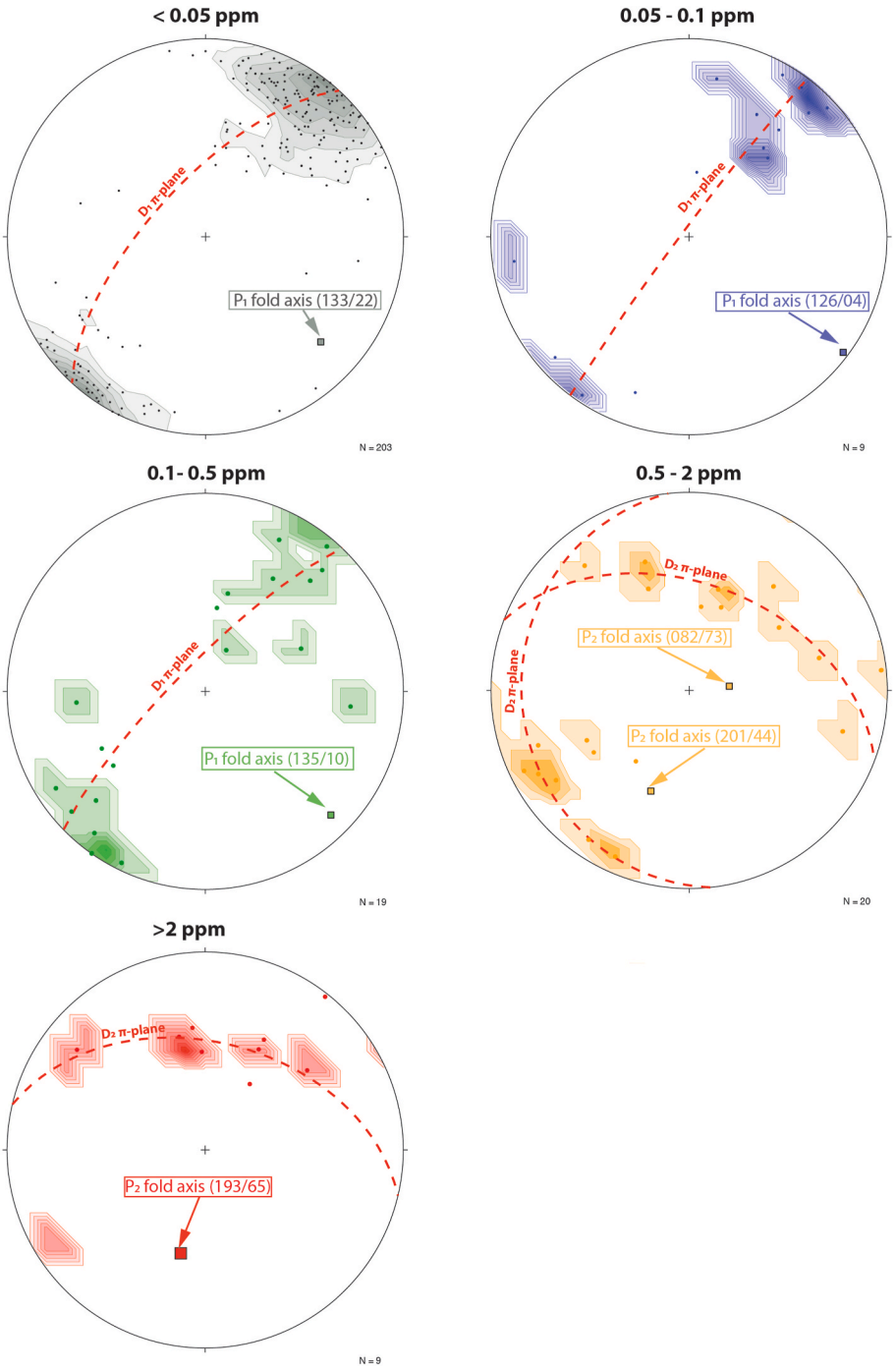

Fig. 15. Stereodiagrams showing the distribution of the poles of $S_{1/0}$ foliation on drill cores from the 2020 drilling campaign for specific gold grade (in ppm).

well documented for several subduction-related orogenic gold deposits from the Alaskan Cordillera, in which the main gold stage occurred during transpressive reactivation of compressive crustal scale faults (Goldfarb et al., 1993, 2008; Goldfarb and Groves, 2015). More recently, Lacroix et al. (2020) reported similar observations within the Los Burros deposits from Central California. These similitudes between different gold deposits worldwide support the hypothesis proposed by Goldfarb et al. (2008) in which the transition from collisional compressive regime to transcurrent deformation is an important mechanism in the formation and maturation of orogenic gold systems. Whereas the role of the transition between pure compression to transcurrent deformation in gold deposition is now undoubtfully documented, the exact physico-chemical mechanisms leading to gold deposition and/or reconcentration remain questionable.

The role of fold interference patterns, and refolding, within the development of ore deposit, and ore-shoot has been already proposed within the Barberton greenstone belt of South Africa (Witt and Ronde, 1994; Jones and Kisters, 2022) in which 85% of the presently and historically mined reefs occur in the hinge region of refolded regional syncline (Jones and Kisters, 2022). Whereas the exact processes leading to ore maturation are not understood yet, these authors acknowledge the control of fluid flow and mineralization during the refolding event. In the case of Boulanger deposit, we infer that D_2 structural overprint linked to the kinematic transition is spatially correlated with the highest gold grade as well as the presence of pyrrhotite.

6.3. Conceptual mechanical model

As discussed above, the transition from pure shortening to transcurrent regime has been documented in several greenstone belts worldwide, including the Guiana Shield, Abitibi Greenstone belts, West and South Africa (e.g., De Ronde and de Wit, 1994; Milesi et al., 1995; Vanderhaeghe et al., 1998; Delor et al., 2003; Hein et al., 2015). Whereas the exact mechanisms conducting to such a transition are still debated (e.g., Gapais et al., 2021), we propose that the passage from pure compressive to transcurrent regimes is a direct response of crustal thickening. Under normal Andersonian conditions (σ vertical = σ_1, σ_2 or σ_3), the development of both sub-horizontal folds (upright fold with horizontal axis) and the quartz-tourmaline vein system as observed at Boulanger deposit require specific stress conditions in which the minimum principal stress, σ_3, is vertical (e.g., Anderson, 1951; Sibson, 1985). Assuming that the vertical stress is exclusively controlled by the thickness of the overburden rock sequence, σ_3 would significantly increase during D_1 crustal thickening event by the development of tight folds and penetrative $S_{1/0}$. Under such conditions, σ_3 continues to increase until it exceeds the intermediate principal stress, σ_2. At that stage, the new stress field orientation conditions, in which σ_3 becomes horizontal and σ_2 vertical, initiate the D_2 transcurrent regime. In a logical manner, such transition should be accompanied by prograde metamorphism (increasing temperature). As described above, the maturation of gold grade during D_2 event is untimely associated with the precipitation of pyrrhotite along space formed by foliation delamination. Whereas the exact composition of pyrrhotite and pyrite have not been investigated in this study, it is relatively well admitted that the pyrite-pyrrhotite transformation occurs in prograde metamorphic conditions (500–550 °C temperature range) (e.g., Zabin and Kremenetskiy, 1993; Groves et al., 2020; Gaboury, 2019). In the case of Boulanger deposit, it is possible that pyrrhotite formed from pyrite present within tuffaceous rocks during crustal thickening event, D_2, which supports the proposed crustal thickening model.

6.4. Implications for mineral exploration

We propose that resolving the geometry of fold interference pattern is fundamental in understanding the distribution of the gold grade at deposit-scale. Indeed, our structural analysis coupled with Au-grade highlights the presence of grade control along the F_2 axial plane formed along refolded D_1 structures such as $S_{1/0}$ foliation and quartz-tourmaline veins. The presence of fold superposition developed within the Rhyacian Paramaca greenstone belt in the location studied here offers new prospective for gold exploration within the Guiana Shield. As suggested by the present study, the gold-grade significantly increases during D_2 fold superposition, with the development of an ore shoot along D_2 axial planes oriented N020. Therefore, we propose that the intersection of D_1 and D_2 mineralized structures may represent favorable zones to investigate. In this context, refining the polyphase fold geometry (e.g., interference pattern) is fundamental. Accordingly, the recognition of the exact fold geometry appears critical for exploration targeting.

7. Conclusions

We report new structural and petrological dataset of the Boulanger gold deposit, hosted within the Rhyacian greenstone belts from the Guiana shield located within the North Guiana Through, French Guiana. The Boulanger deposit is characterized by a complex polyphase deformation and mineralization history involving a coaxial shortening phase, D_1, followed by a transcurrent deformation event, D_2. The main ore bodies consist of a typical orogenic gold deposit associated with the emplacement of quartz-tourmaline-pyrite-carbonate extension and shear veins in response to NNE-SSW compressive event (D_1). This shortening event is followed by transcurrent deformation, D_2. Locally, D_2 is expressed by the formation of N020-030 narrow zones (F_2 axial trace) along which D_1 structures are reoriented. The structural analysis performed on both $S_{1/0}$ foliation and on geophysical data interpretation highlights the presence of Type-1 interference patterns. These zones are associated with significant gold enrichment and the apparition of a new ore assemblage dominated by pyrrhotite-pyrite. Quantitative structural analysis approach, based on measured foliations ($S_{1/0}$) and gold grade demonstrates that D_2-related folding is associated with important gold endowment. These findings suggest that the characterization of the exact fold interference pattern is fundamental for the targeting of favorable enriched zones at the deposit scale.

CRediT authorship contribution statement

Brice Lacroix: Writing – review & editing, Writing – original draft, Validation, Resources, Project administration, Methodology, Investigation, Funding acquisition, Formal analysis, Data curation, Conceptualization. **Dennis Lahondes:** Writing – review & editing, Resources, Project administration, Investigation. **Pierre-Jean Hainque:** Writing – review & editing, Validation. **Etienne Le Goff:** Supervision, Resources, Project administration. **Dominique Fournier:** Writing – original draft, Project administration, Investigation, Funding acquisition, Formal analysis. **Alix Hauteville:** Visualization, Investigation. **Blandine Gourcerol:** Conceptualization. **Aurélien Eglinger:** Writing – review & editing. **Anne-Sylvie Andre-Mayer:** Writing – review & editing.

Declaration of competing interest

The authors declare the following financial interests/personal relationships which may be considered as potential competing interests: Brice Lacroix reports financial support was provided by Kansas State University. Brice Lacroix reports travel was provided by Reunion Gold Corporation.

Data availability

Data will be made available on request.

Acknowledgments

Financial and logistical support was also provided by Reunion Gold Corporation (Québec, Canada) and Kansas State University (Manhattan KS, USA). This study benefited greatly from additional geological mapping, core logging and structural data made available to us by Reunion Gold Corporation. We are grateful to the exploration geologist team at Boulanger, and Justin Van der torn for suggestions to improve the English. We thank Journal of South American Earth Sciences editor M. da Costa Pereira Lavalle Heilbron, G. Pires and an anonymous reviewer for their constructive comments that helped to improve this manuscript.

References

Adagunodo, T.A., Sunmonu, L.A., Adeniji, A.A., 2015. An Overview of Magnetic Method in Mineral Exploration.
Anderson, E.M., 1951. The Dynamics of Faulting and Dyke Formation with Application to Britain, second ed. Oliver and Boyd, Edinburgh, p. 206.
Avelar, V.G., Lafon, J.M., Delor, C., Guerrot, C., Lahondère, D., 2003. Archean crustal remnants in the easternmost part of the Guiana Shield: Pb/Pb and Sm/Nd geochronological evidence for Mesoarchean versus Neoarchean signatures. Géologie de la France 2e3e4, 83e100.
Barreto, C.J.S., Lafon, J.M., da Rosa Costa, L.T., Dantas, E.L., 2013. Paleoproterozoic granitoids from the northern limit of the Archean Amapá block (Brazil), Southeastern Guyana Shield: Pb–Pb evaporation in zircons and Sm–Nd geochronology. J. S. Am. Earth Sci. 45, 97–116.
Bons, P.D., Elburg, M.A., Gomez-Rivas, E., 2012. A review of the formation of tectonic veins and their microstructures. J. Struct. Geol. 43, 33–62.
Chauvet, A., 2019. Structural control of ore deposits: the role of pre-existing structures on the formation of mineralised vein systems. Minerals 9 (1), 56.

Clegg, P., Holdsworth, R.E., 2005. Complex deformation as a result of strain partitioning in transpression zones: an example from the Leinster Terrane, SE Ireland. J. Geol. Soc. 162 (1), 187–202.
Combes, V., Eglinger, A., André-Mayer, A.S., Teitler, Y., Heuret, A., Gibert, P., Béziat, D., 2021. Polyphase Gold Mineralization at the Yaou Deposit, French Guiana.
Combes, V., Eglinger, A., André-Mayer, A.S., Teitler, Y., Jessell, M., Zeh, A., Reisberg, L., Heuret, A., Gibert, P., 2022. Integrated geological-geophysical investigation of gold-hosting Rhyacian intrusions (Yaou, French Guiana), from deposit-to district-scale. J. S. Am. Earth Sci. 114, 103708.
Cox, S.F., Wall, V.J., Etheridge, M.A., Potter, T.F., 1991. Deformational and metamorphic processes in the formation of mesothermal vein-hosted gold deposits—examples from the Lachlan Fold Belt in central Victoria, Australia. Ore Geol. Rev. 6 (5), 391–423.
Daoust, C., Voicu, G., Brisson, H., Gauthier, M., 2011. Geological setting of the paleoproterozoic rosebel gold district, Guiana shield, Suriname. J. S. Am. Earth Sci. 32 (3), 222–245.
de Ronde, C.E., de Wit, M.J., 1994. Tectonic history of the Barberton greenstone belt, South Africa: 490 million years of Archean crustal evolution. Tectonics 13 (4), 983–1005.
Delor, C., de Roever, E.W.F., Lafon, J.-M., Lahondere, D., Rossi, P., Cocherie, A., Guerrot, C., Potrel, A., 2003a. The Bakhuis ultrahigh-temperature granulite belt (Suriname) : II. Implications for late Transamazonian crustal stretching in a revised. Geol. Fr. 2–3– _4, 207–230.
Delor, C., Lahondere, D., Egal, E., Lafon, J.-M., Cocherie, A., Guerrot, C., Rossi, P., Truffert, C., Theveniaut, H., Phillips, D., Avelar, V.G.d., 2003b. 2-3-4 In: transamazonian crustal growth and reworking as revealed by the 1:500000 scale geological map of French Guiana. Geol. Fr. 5–57.
Dubé, B., Gosselin, P., Mercier-Langevin, P., Hannington, M., Galley, A., 2007. Gold-rich volcanogenic massive sulphide deposits. Geological Association of Canada, Mineral Deposits Division 75–94.
Fagereng, Å., Remitti, F., Sibson, R.H., 2010. Shear veins observed within anisotropic fabric at high angles to the maximum compressive stress. Nat. Geosci. 3 (7), 482–485.
Fossen, H., Cavalcante, G.C.G., Pinheiro, R.V.L., Archanjo, C.J., 2019. Deformation–progressive or multiphase? J. Struct. Geol. 125, 82–99.
Gaboury, D., 2019. Parameters for the formation of orogenic gold deposits. B. Appl. Earth Sci. 128 (3), 124–133.
Gapais, D., Alimoenadi, G., Balraadjsing, N., Poupeau, B., 2021. The Rosebel gold mining district (Trans-Amazonian belt, Suriname), a new structural framework. Bull. Soc. Geol. Fr. 192 (1).
Goldfarb, R.J., Groves, D.I., 2015. Orogenic gold: common or evolving fluid and metal sources through time. Lithos 233, 2–26.
Goldfarb, R.J., Snee, L.W., Pickthorn, W.J., 1993. Orogenesis, high-T thermal events, and gold vein formation within metamorphic rocks of the Alaskan Cordillera. Mineral. Mag. 57 (388), 375–394.
Goldfarb, R.J., Groves, D.I., Gardoll, S., 2001. Orogenic gold and geologic time: a global synthesis. Ore Geol. Rev. 18 (1–2), 1–75.
Goldfarb, R.J., Baker, T., Dubé, B., Groves, D.I., Hart, C.J., Gosselin, P., 2005. Distribution, Character, and Genesis of Gold Deposits in Metamorphic Terran.
Goldfarb, R.J., Hart, C.J., Marsh, E.E., 2008. Orogenic gold and evolution of the Cordilleran orogen. Ores and orogenesis: Circum-Pacific tectonics, geologic evolution, and ore deposits: Arizona Geological Society Digest 22, 311–323.
Groves, D.I., Goldfarb, R.J., Gebre-Mariam, M., Hagemann, S.G., Robert, F., 1998. Orogenic gold deposits: a proposed classification in the context of their crustal distribution and relationship to other gold deposit types. Ore Geol. Rev. 13 (1–5), 7–27.
Groves, D.I., Santosh, M., Deng, J., Wang, Q., Yang, L., Zhang, L., 2020. A holistic model for the origin of orogenic gold deposits and its implications for exploration. Miner. Deposita 55, 275–292.
Guiraud, J., Tremblay, A., Jébrak, M., Ross, P.S., Lefrançois, R., 2020. Stratigraphic setting and timing of the Montagne d'Or deposit, a unique Rhyacian Au-rich VMS deposit of the Guiana Shield, French Guiana. Precambrian Res. 337, 105551.
Gurin, G., Ilyin, Y., Nilov, S., Ivanov, D., Kozlov, E., Titov, K., 2018. Induced polarization of rocks containing pyrite: interpretation based on X-ray computed tomography. J. Appl. Geophys. 154, 50–63.
Hein, K.A.A., Matsheka, I.R., Bruguier, O., Masurel, Q., Bosch, D., Caby, R., Monie, P., 2015. The Yatela gold deposit: 2 billion years in the making. J. Afr. Earth Sci. 112, 548–569.
Jébrak, M., Heuret, A., Rostan, P., 2021. The gold, peoples and multiple frontiers of French Guiana. Extr. Ind. Soc. 8 (1), 8–22.
Jones, C., Kisters, A., 2022. Regional and local controls of hydrothermal fluid flow and gold mineralization in the Sheba and Fairview mines, Barberton Greenstone Belt, South Africa. Ore Geol. Rev. 144, 104805.
Kroonenberg, S.B., De Roever, E.W.F., Fraga, L.M., Reis, N.J., Faraco, T., Lafon, J.M., Cordani, U., Wong, T.E., 2016. Paleoproterozoic evolution of the Guiana Shield in Suriname: a revised model. Neth. J. Geosci. 95 (4), 491–522.
Labaume, P., Berty, C., Laurent, P.H., 1991. Syn-diagenetic evolution of shear structures in superficial nappes: an example from the Northern Apennines (NW Italy). J. Struct. Geol. 13 (4), 385–398.
Lacroix, B., Leclère, H., Buatier, M., Fabbri, O., 2013. Weakening processes in thrust faults: insights from the M onte P erdido thrust fault (southern P yrenees, S pain). Geofluids 13 (1), 56–65.
Lacroix, B., Hughes, J., Lahfid, A., Spangenberg, J.E., Putlitz, B., Ward, C., Niemi, N., Kempton, P.D., 2020. Structure and origin of the gold mineralization in the nacimiento block: the Los Burros deposits (central California). Ore Geol. Rev. 125, 103668.
Lasserre, J.L., Ledru, P., Manier, E., Mercier, D., 1989. Le Prot6rozoïque inférieur de Guyane. Révision lithostructurale. Implications pour la formation déritique ORAPU et la gitologie de l'or. Unpubl. Rep. BRGM-ENSMP 89 GUF 023:56.
Ledru, P., Pons, J., Milési, J.P., Feybesse, J.L., Johan, V., 1991. Transcurrent tectonics and polycyclic evolution in the Lower Proterozoic of Senegal-Mali. Precambrian Res. 50 (3–4), 337–354.
Masurel, Q., Eglinger, A., Thébaud, N., Allibone, A., André-Mayer, A.S., McFarlane, H., Miller, J., Jessell, M., Aillères, L., Vanderhaeghe, O., Salvi, S., 2022. Paleoproterozoic gold events in the southern West African Craton: review and synopsis. Miner. Deposita 57 (4), 513–537.
Milesi, J.-P., Egal, E., et al., 1995. Les minéralisations du Nord de la Guyane française dans leur cadre géologique. Chron. Rech. Min. 518, 5–59.
Milesi, J., Lerouge, C., Delor, C., Ledru, P., Billa, M., Cocherie, A., Egal, E., Fouillac, A., Lahondere, D., Lasserre, J., Marot, A., Martel-Jantin, B., Rossi, P., Tegyey, M., Theveniault, H., Thieblemont, D., Vanderhaeghe, O., 2003. Gold deposits (gold-bearing tourmalinites, gold-bearing conglomerates, and mesothermal lodes), markers of the geological evolution of French Guiana: geology, metallogeny, and stable isotope constraints. Geol. Fr. 2–3–4, 257–290.
Neumayr, P., Ridley, J.R., McNaughton, N.J., Kinny, P.D., Barley, M.E., Groves, D.I., 1998. Timing of gold mineralization in the Mt York district, Pilgangoora greenstone belt, and implications for the tectonic and metamorphic evolution of an area linking the western and eastern Pilbara Craton. Precambrian Res. 88 (1–4), 249–265.
Perret, J., Eglinger, A., André-Mayer, A.S., Aillères, L., Feneyrol, J., Hartshorne, C., Abanyin, E., Bosc, R., 2020. Subvertical, linear and progressive deformation related to gold mineralization at the Galat Sufar South deposit, Nubian Shield, NE Sudan. J. Struct. Geol. 135, 104032.
Phillips, G.N., Powell, R., 2010. Formation of gold deposits: a metamorphic devolatilization model. J. Metamorph. Geol. 28 (6), 689–718.
Poulsen, K.H., 2000. Geological classification of Canadian gold deposits. Bull. Geol. Surv. Can. 540, 1–106.
Ramsay, J.G., 1967. Folding and Fracturing of Rocks. Mc Graw Hill Book Company, p. 568.
Santos, J.O.S., Hartmann, L.A., Gaudette, H.E., Groves, D.I., Mcnaughton, N.J., Fletcher, I.R., 2000. A new understanding of the provinces of the Amazon Craton based on integration of field mapping and U-Pb and Sm-Nd geochronology. Gondwana Res. 3 (4), 453–488.
Sibson, R.H., 1985. A note on fault reactivation. J. Struct. Geol. 7 (6), 751–754.
Sibson, R.H., 2020. Preparation zones for large crustal earthquakes consequent on fault-valve action. Earth Planets Space 72, 1–20.
Sumner, J.S., 2012. Principles of Induced Polarization for Geophysical Exploration. Elsevier.
Tassinari, C.C., Munhá, J.M., Teixeira, W., Palácios, T., Nutman, A.P., Sosa, C., Santos, A. P., Calado, B.O., 2004. The Imataca Complex, NW Amazonian Craton, Venezuela: crustal evolution and integration of geochronological and petrological cooling histories. Episodes Journal of International Geoscience 27 (1), 3–12.
Tedeschi, M., Hagemann, S.G., Davis, J., 2018. The Karouni gold deposit, Guyana, South America: Part I. Stratigraphic setting and structural controls on mineralization. Econ. Geol. 113 (8), 1679–1704.
Tedeschi, M.T., Hagemann, S.G., Kemp, A.I.S., Kirkland, C.L., Ireland, T.R., 2020. Geochronological constrains on the timing of magmatism, deformation and mineralization at the Karouni orogenic gold deposit: Guyana, South America. Precambrian Res. 337, 105329.
Thébaud, N., Sugiono, D., LaFlamme, C., Miller, J., Fisher, L., Voute, F., Tessalina, S., Sonntag, I., Fiorentini, M., 2018. Protracted and polyphased gold mineralisation in the Agnew district (Yilgarn craton, Western Australia). Precambrian Res. 310, 291–304.
Tomkins, A.G., Mavrogenes, J.A., 2002. Mobilization of gold as a polymetallic melt during pelite anatexis at the Challenger deposit, South Australia: a metamorphosed Archean gold deposit. Econ. Geol. 97 (6), 1249–1271.
Van Noten, K., Muchez, P., Sintubin, M., 2011. Stress-state evolution of the brittle upper crust during compressional tectonic inversion as defined by successive quartz vein types (High-Ardenne slate belt, Germany). J. Geol. Soc. 168 (2), 407–422.
Vanderhaeghe, O., Ledru, P., Thiéblemont, D., Egal, E., Cocherie, A., Tegyey, M., Milési, J.P., 1998. Contrasting mechanism of crustal growth: geodynamic evolution of the Paleoproterozoic granite–greenstone belts of French Guiana. Precambrian Res. 92 (2), 165–193.
Voisey, C.R., Willis, D., Tomkins, A.G., Wilson, C.J., Micklethwaite, S., Salvemini, F., Bougoure, J., Rickard, W.D., 2020. Aseismic refinement of orogenic gold systems. Econ. Geol. 115 (1), 33–50.
Zhabin, A.G., Kremenetskiy, A.A., 1993. The pyrite-pyrrhotite transformation as an ore-concentrating geochemical barrier. Int. Geol. Rev. 35 (4), 359–368.